



Combination anti-CTLA-4 plus anti-PD-1 checkpoint blockade utilizes cellular mechanisms partially distinct from monotherapies

Spencer C. Wei^a, Nana-Ama A. S. Anang^a, Roshan Sharma^{b,c}, Miles C. Andrews^d, Alexandre Reuben^d, Jacob H. Levine^b, Alexandria P. Cogdill^{a,d}, James J. Mancuso^a, Jennifer A. Wargo^{c,d,e}, Dana Pe'er^{b,f}, and James P. Allison^{a,g,1}

^aDepartment of Immunology, The University of Texas MD Anderson Cancer Center, Houston, TX 77030; ^bComputational and Systems Biology Program, Sloan Kettering Institute, New York, NY 10065; ^cDepartment of Applied Physics and Applied Mathematics, Columbia University, New York, NY 10027; ^dDepartment of Surgical Oncology, The University of Texas MD Anderson Cancer Center, Houston, TX 77030; ^eDepartment of Genomic Medicine, The University of Texas MD Anderson Cancer Center, Houston, TX 77030; ^fParker Institute for Cancer Immunotherapy, Memorial Sloan Kettering Cancer Center, New York, NY 10065; and ^gParker Institute for Cancer Immunotherapy, The University of Texas MD Anderson Cancer Center, Houston, TX 77030

Contributed by James P. Allison, September 13, 2019 (sent for review January 2, 2019; reviewed by Rafi Ahmed and Mario Sznoł)

Immune checkpoint blockade therapy targets T cell-negative costimulatory molecules such as cytotoxic T lymphocyte antigen-4 (CTLA-4) and programmed cell death-1 (PD-1). Combination anti-CTLA-4 and anti-PD-1 blockade therapy has enhanced efficacy, but it remains unclear through what mechanisms such effects are mediated. A critical question is whether combination therapy targets and modulates the same T cell populations as monotherapies. Using a mass cytometry-based systems approach, we comprehensively profiled the response of T cell populations to monotherapy and combination anti-CTLA-4 plus anti-PD-1 therapy in syngeneic murine tumors and clinical samples. Most effects of monotherapies were additive in the context of combination therapy; however, multiple combination therapy-specific effects were observed. Highly phenotypically exhausted cluster of differentiation 8 (CD8) T cells expand in frequency following anti-PD-1 monotherapy but not combination therapy, while activated terminally differentiated effector CD8 T cells expand only following combination therapy. Combination therapy also led to further increased frequency of T helper type 1 (Th1)-like CD4 effector T cells even though anti-PD-1 monotherapy is not sufficient to do so. Mass cytometry analyses of peripheral blood from melanoma patients treated with immune checkpoint blockade therapies similarly revealed mostly additive effects on the frequencies of T cell subsets along with unique modulation of terminally differentiated effector CD8 T cells by combination ipilimumab plus nivolumab therapy. Together, these findings indicate that dual blockade of CTLA-4 and PD-1 therapy is sufficient to induce unique cellular responses compared with either monotherapy.

immunotherapies. It is possible that combination therapies act through modulation of the same cellular populations as constituent monotherapies. Alternatively, combination therapies, particularly those that have convergent effects at the cellular or molecular level,

Significance

Immune checkpoint blockade therapy has become a critical pillar of cancer therapy. Here, we characterize the cellular mechanisms of monotherapy and combination anti-cytotoxic T lymphocyte antigen-4 plus anti-programmed cell death-1 therapy. Using high-dimensional single-cell profiling, we determine that combination therapy elicits cellular responses that are partially distinct from those induced by either monotherapy. In particular, combination therapy mediates a switch from expansion of phenotypically exhausted cluster of differentiation 8 (CD8) T cells to expansion of activated effector CD8 T cells. In addition, we systematically compare T cell subsets present in matched peripheral blood and tumor tissues to define what aspects of antitumor responses can be observed peripherally. These findings have significant implications for both the cellular mechanisms of action and biomarkers of response to monotherapies and combination therapy.

Author contributions: S.C.W., D.P., and J.P.A. designed research; S.C.W. and N.A.S.A. performed research; R.S., J.H.L., and D.P. contributed new reagents/analytic tools; S.C.W., R.S., M.C.A., A.R., A.P.C., J.J.M., J.A.W., D.P., and J.P.A. analyzed data; S.C.W. and J.P.A. wrote the paper; and A.P.C. provided technical assistance.

Reviewers: R.A., Emory University; and M.S., Yale University.

Competing interest statement: S.C.W. is currently an employee of Spotlight Therapeutics. J.P.A. is a cofounder of Jounce and Neon Therapeutics. J.P.A. has ownership interest in Jounce Therapeutics, Neon Therapeutics, Forty Seven, ImaginAb, Marker Therapeutics, Tvardi, Constellation, BioAtla, Polaris, and Apricity; is a scientific advisory board member/consultant for Jounce, BioAtla, Neon, Amgen, Forty Seven, ImaginAb, Marker Therapeutics, Apricity, Polaris, Oncolytics, and Pieris; and has received royalties from intellectual property licensed to BMS and Merck. M.C.A. reports travel support and honoraria from Merck unrelated to the current work. J.A.W. is a paid speaker for Imedex, Dava Oncology, Omniprex, Illumina, Gilead, MedImmune, and Bristol Meyers Squibb. J.A.W. is a consultant/advisory board member for Roche-Genentech, Novartis, Astra-Zeneca, Glaxo Smith Klein, Bristol Meyers Squibb, Merck, and Microbiome DX. J.A.W. also receives clinical trial support from Glaxo Smith Klein, Roche-Genentech, Bristol Meyers Squibb, and Novartis. J.A.W. is a clinical and scientific advisor at Microbiome DX and a consultant at Biothera Pharma, Merck Sharp, and Dohme. J.A.W. is an inventor on a US patent application submitted by The University of Texas MD Anderson Cancer Center that covers methods to enhance checkpoint blockade therapy by the microbiome. Reviewer R.A. holds patents on programmed cell death-1-targeted cancer therapies.

This open access article is distributed under [Creative Commons Attribution-NonCommercial-NoDerivatives License 4.0 \(CC BY-NC-ND\)](https://creativecommons.org/licenses/by-nc-nd/4.0/).

Data deposition: Mass cytometry data have been deposited in the Flow Repository (murine TIL data; repository ID: [FR-FCM-ZYQQ](https://flowrepository.org/repo/FR-FCM-ZYQQ)). Human peripheral blood data were also deposited in the Flow Repository (repository ID: [FCM-FR-ZYQR](https://flowrepository.org/repo/FCM-FR-ZYQR)).

¹To whom correspondence may be addressed. Email: jallison@mdanderson.org.

This article contains supporting information online at www.pnas.org/lookup/suppl/doi:10.1073/pnas.1821218116/-DCSupplemental.

First published October 21, 2019.

CTLA-4 | PD-1 | immune checkpoint blockade | mass cytometry | T cell

Immune checkpoint blockade can induce long-term durable responses; however, these remarkable responses are limited to a minority of patients (1–3). One of the promising approaches to improve the scope and efficacy of these therapies is combinatorial therapy. There are over 1,100 clinical trials currently testing the efficacy of programmed cell death-1 (PD-1) blockade agents in combination with other therapies (4). These include over 250 combining therapeutic agents targeting cytotoxic T lymphocyte antigen-4 (CTLA-4) and PD-1, as well as combinations with or of novel agents targeting other T cell costimulatory molecules (e.g., TIM-3, LAG3, OX40). Additionally, combinations of immune checkpoint blockade with other therapeutic modalities such as radiation, chemotherapy, and targeted therapies are under active investigation. These efforts are hampered, however, by our limited understanding of the underlying biological mechanisms. In particular, it remains unclear in many cases what precise molecular events and cellular populations are modulated by checkpoint blockade. It is clear that mechanistic insights are necessary to guide rational design of combination therapies. We sought to define what information is needed to guide such rational design of

IMMUNOLOGY AND INFLAMMATION

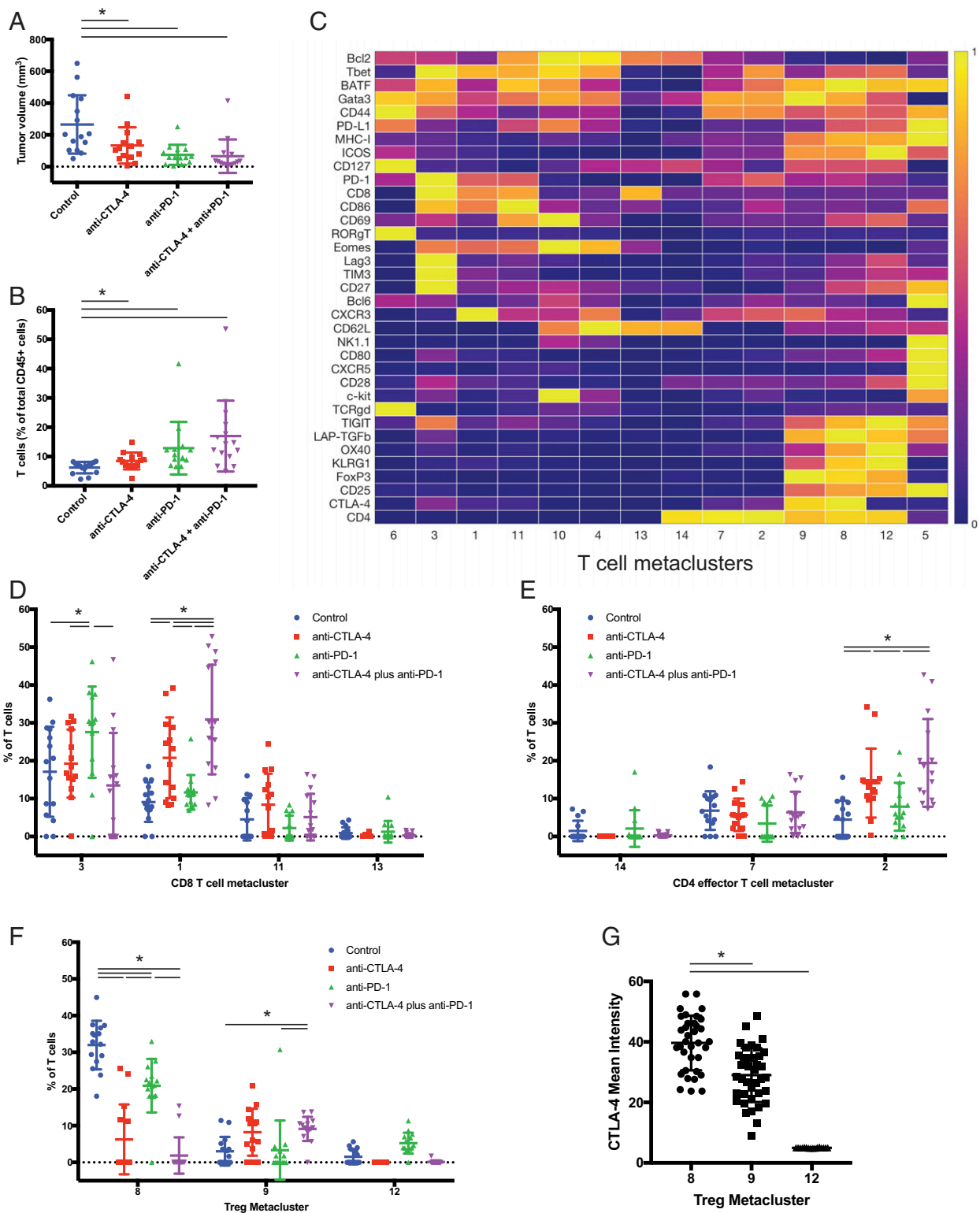


Fig. 1. Combination anti-CTLA-4 plus anti-PD-1 therapy differentially affects MC38 tumor-infiltrating T cell populations. (A) MC38 tumor volumes 13 d after tumor inoculation are displayed from mice treated with control, monotherapy, or combination anti-CTLA-4 plus anti-PD-1 therapy. (B) T cell frequency as a percentage of total MC38 tumor-infiltrating CD45⁺ cells. (C) Heat map of MC38 tumor-infiltrating T cell metaclusters displaying expression values of individual parameters normalized to the maximum mean value across metaclusters. (D) Relative frequency of CD8 T cell metaclusters. (E) Relative frequency of CD4 effector T cell metaclusters. (F) Relative frequency of Treg metaclusters. (G) Mean intensity of CTLA-4 of Treg metaclusters. Each data point reflects the mean intensity of the individual clusters associated with the metaclusters. Data are pooled from 3 biological replicate cohorts and are displayed on a per mouse basis. Mean and SD are displayed. **P* < 0.05, 2-tailed *t* test with Welch's correction. (See also *SI Appendix*, Fig. S1.)

In the Treg compartment, both anti-CTLA-4 and anti-PD-1 monotherapies led to decreased relative frequencies of specific subsets and combination therapy led to additive reductions in Treg frequencies (Fig. 1E). These decreases likely constitute both Fc-mediated cell depletion and relative dilution, as anti-CTLA-4 treatment leads to Treg depletion in murine tumor models (21–23). Here, the anti-CTLA-4 antibody clone 9H10, which can mediate Treg depletion in murine tumor models, was utilized in both monotherapy and combination therapy. Similar experiments in murine tumor models using nondepleting anti-CTLA-4 antibodies may help to further define the contributions of direct effects on T effector cells and Treg depletion. Notably, however, while specific anti-CTLA-4 antibody clones can mediate Treg depletion in murine tumor models, recent evidence indicates that ipilimumab therapy does not lead to Treg depletion in humans (24). Interestingly, however, the frequency of only specific Treg populations decreased following both monotherapy and combination therapy (Fig. 1F). This may be explained by differential sensitivity of these populations to antibody-dependent cellular cytotoxicity (ADCC) efficiency or, alternatively, differential effects on the proliferation of specific Treg populations due to checkpoint blockade. Notably, these are not mutually exclusive possibilities but do reflect fundamentally different mechanistic explanations.

We investigated whether different Treg populations expressed varying levels of CTLA-4 as a potential explanation for varying sensitivities to blockade. Treg metacluster 8 expressed the highest levels of CTLA-4 and displayed the most dramatic decrease in frequency following CTLA-4 blockade (Fig. 1F and G). Interestingly, however, Treg metacluster 9 expressed significant but slightly lower levels of CTLA-4 than metacluster 8, yet did not decrease in frequency following either anti-CTLA-4 or combination therapy. Furthermore, Treg metacluster 12 did not express detectable levels of CTLA-4 but did decrease in frequency following anti-CTLA-4 and combination therapies (Fig. 1F and G). This suggests that modulation of metacluster 12 is mediated by indirect effects or by low amounts of CTLA-4 below the limit of detection.

Together, these data reveal that relative to monotherapies, the effects of combination therapy fall into discrete groups, including opposing effects on phenotypically exhausted CD8 T cells, additive expansion of Th1-like CD4 effector T cells, and decreases in specific types of Tregs. Similar effects on the relative frequency of T cell subsets as a frequency of total CD45⁺ tumor-infiltrating cells support the notion that these changes reflect increases in population, rather than simply relative changes contained only within the T cell compartment (*SI Appendix, Fig. S1E*). In addition, these data raise the possibility that combination therapy may have unique biological effects on T cell function. Notably, the analysis of total T cells was not sufficient to detect differences between combination and monotherapies (Fig. 1B), while unsupervised phenotypic classification enabled the detection of relevant biological differences (Fig. 1C–F). From a mechanistic perspective, such subsets can arise due to modulated proliferation, but also changes in differentiation. Consistent with this possibility, negative costimulation restricts the boundaries of T cell phenotypes achieved through peripheral differentiation (25). In addition, checkpoint blockade can lead to proliferative expansion of specific T cell subsets, but these cells can differentiate and display altered phenotypes when detected at later times. For example, PD-1 blockade leads to expansion of TCF1⁺ CD8 T cells with memory and stem-like properties, which contributes to the increased frequency of differentiated PD-1⁺ CD8 T cells in the periphery (26–28).

The Frequencies of Specific Tumor-Infiltrating T Cell Populations Correlate with Response in the Contexts of Monotherapy and Combination Checkpoint Blockade Therapy. We next sought to gain insight into whether differential effects on T cell subset

frequency due to monotherapy and combination therapy reflect functional changes with respect to tumor rejection. We assessed the correlation between individual populations and tumor volume. In the case of most T cell subsets, findings were similar to prior observations using similar methods (15) (Fig. 2A–C and *SI Appendix, Fig. S2A and B*). For example, the frequency of Th1-like CD4 effector T cells negatively correlated with tumor volume, consistent with prior findings and a functional role in tumor rejection (15) (Fig. 2B, metacluster 2). It is unclear whether combination therapy differentially modulates the activity of this subset compared with anti-CTLA-4 monotherapy (which also leads to an increase in frequency). The functional contribution of this population is not well defined, but may contribute to tumor rejection through several mechanisms such as enhancing CD8 T cell infiltration, increasing antigen presentation, or direct tumor lysis.

The frequency of Treg metacluster 8 positively correlated with tumor volume, consistent with a protumor functional role (Fig. 2C). The frequency of activated effector CD8 T cells (metacluster 1) negatively correlated with tumor volume (Fig. 2A). Thus, this population has a functional role independent of therapy, but only combination therapy leads to an increase in frequency. All T cell populations had a similar correlative relationship with tumor volume in comparison to prior findings in the context of monotherapies, with the notable exception of metacluster 3. The frequency of phenotypically exhausted PD-1^{high} Lag3⁺ Tim3⁺ CD8 T cells (metacluster 3) did not significantly correlate with tumor volume. At first, this appears to contrast with the notion that exhausted CD8 T cells retain functional capacity as well as prior findings that this population negatively correlates with tumor volume in preclinical tumor models (15). However, upon further inspection, the correlations between the frequency of metacluster 3 and tumor volume diverge in the contexts of monotherapies and combination therapy (*SI Appendix, Fig. S2B*). While a strong negative correlation was observed in the context of monotherapy, consistent with prior observations, a positive correlation was observed in the context of combination therapy. This suggests that metacluster 3 has distinct effects on antitumor immune responses in the context of monotherapy and combination therapy.

The striking differences in the frequencies and functional associations of phenotypically exhausted and activated effector CD8 T cells (metaclusters 3 and 1, respectively) in the context of monotherapy versus combination therapy raise several interesting nonmutually exclusive possibilities. First, combination therapy may be able to prevent CD8 T cells from acquiring a fully exhausted phenotype. It is also possible that combination therapy may be sufficient to reverse T cell exhaustion, although this is unlikely, given the kinetics of these experiments and recent evidence that epigenetic programs enforce an exhausted cell state (29, 30). Second, the enhanced CD28 costimulation enabled by CTLA-4 blockade may enhance priming and repriming of newly activated as well as already activated T cells, delaying or perhaps preventing induction of T cell exhaustion. Finally, combination therapy may have distinct effects on the proliferative capacity of specific T cell populations that manifest as differences in relative frequency.

We next investigated whether differences in the efficacy of therapy (and thus the “T cell inflammation status”) could explain the apparent switch from expansion of phenotypically exhausted cells to expansion of newly activated cells. Taking advantage of the biological variance in this model system, we compared approximately size-matched tumors of monotherapy and combination therapy groups, observing similar effects on CD8 T cell populations in response to monotherapies and combination therapy (*SI Appendix, Fig. S2D and E*). This suggests that differences in efficacy do not underlie the differential effects on CD8 T cell metacluster 1 and 3 subsets, although it remains possible that the kinetics of antitumor responses may be regulated in a treatment-dependent manner. To investigate whether monotherapies and combination therapy differentially modulate

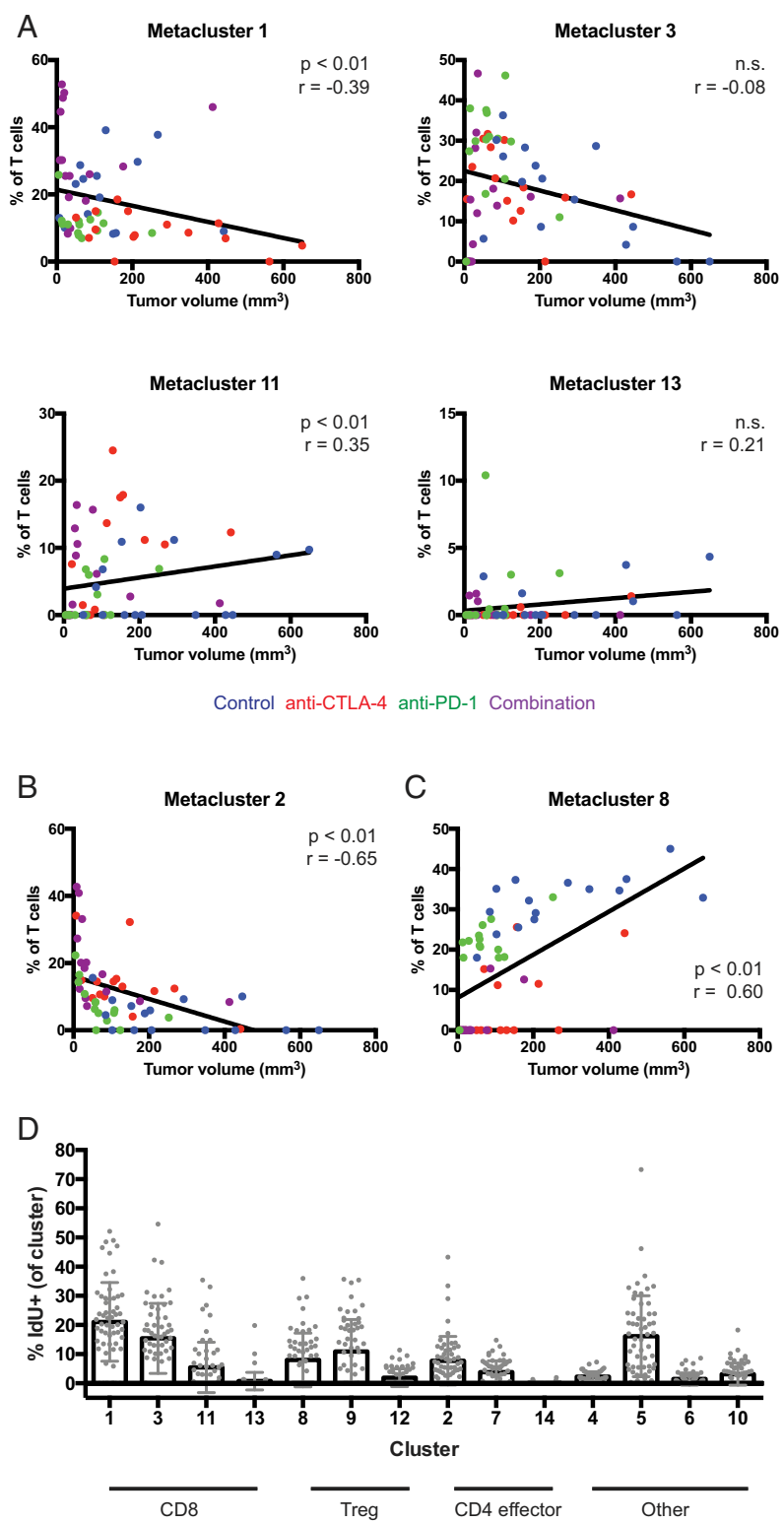


Fig. 2. Correlative relationships between MC38 tumor growth and T cell subset frequency. (A) Relative frequency of denoted MC38 tumor-infiltrating T cell metaclusters plotted as a function of final tumor volume on day 13 postinoculation. Data from all treatment groups are displayed together. Data are pooled from the 3 biological replicate cohorts analyzed in Fig. 1 and are displayed on a per mouse basis. Data points are color-coded by treatment: control (blue), anti-CTLA-4 (red), anti-PD-1 (green), and combination (purple). n.s., not significant. (B) Relative frequency of Th1-like CD4 effector cells (metacluster 2) plotted as a function of final tumor volume. Data from all treatment groups are displayed together. (C) Relative frequency of regulatory T cells (metacluster 8) plotted as a function of final tumor volume. Data from all treatment groups are displayed together. (D) Frequency of IdU⁺ T cells is displayed for each MC38 tumor-infiltrating T cell metacluster on a per mouse basis. The mean and SD are displayed. Linear regression lines are displayed along with Spearman r and P values. (See also *SI Appendix, Fig. S2.*)

proliferation of tumor-infiltrating T cell populations, we assessed short-term iodo-deoxyuridine (IdU) incorporation to identify differences in cellular proliferation between tumor-infiltrating T cell subsets (*Methods*). Consistent with previous findings (15), tumor-infiltrating T cell subsets displayed a wide range of proliferative activity (Fig. 2D). No differences in the proliferation of phenotypically exhausted CD8 T cells were observed between treatment groups (*SI Appendix, Fig. S2E*), which indicates that the decrease in frequency in response to combination therapy is not due to modulation of proliferation. Interestingly, despite displaying a highly exhausted phenotype, nearly 20% of PD-1^{high} Lag3⁺ Tim3⁺ CD8 T cells (metacluster 3) were actively proliferating regardless of therapy. These data support a model in which phenotypically exhausted CD8 T cells still functionally contribute to antitumor responses (Fig. 2A and *SI Appendix, Fig. S2B*).

The shift from phenotypically exhausted to activated effector CD8 T cell effects following combination therapy may be exerted through multiple mechanisms, including modulation of T cell trafficking to the tumor, altered T cell survival, or preventing the adoption of a fully exhausted state. Inhibition of lymphocyte egress from secondary lymphoid organs leads to a loss of therapeutic efficacy in the context of anti-PD-1 with intratumoral adjuvants (31), consistent with the necessity of engagement of peripheral T cells in secondary lymphoid organs for therapeutic efficacy. Notably, however, inhibition of lymphocyte egress attenuates responses to immune checkpoint blockade combination therapies when performed during early phases of responses to therapy but not when performed later (32). This suggests that combination immune checkpoint blockade enhances T cell infiltration and also modulates the functional responses of T cells already within the tumor microenvironment (TME).

Comparison of T Cell Populations in Peripheral Blood from Melanoma Patients Treated with Monotherapies versus Ipilimumab Plus Nivolumab Combination Therapy. We next sought to understand whether such mechanistic differences underlie responses to monotherapies and combination immune checkpoint blockade therapy in humans. Prior studies indicate that significant changes in the frequencies of CD8 T cell and other immune cell populations can be observed in peripheral blood of patients receiving anti-PD-1 therapy (33–35). Identifying peripheral blood immune cell populations that are modulated by monotherapy and combination therapy might provide candidate biomarkers of response or pharmacokinetics, regardless of whether such phenotypes are present within the tumor. Based on our preclinical studies, we sought to determine whether analyses of peripheral blood could provide insights into the cellular effects of combination therapy. We analyzed peripheral blood samples from a retrospective cohort of metastatic melanoma patients treated with ipilimumab, anti-PD-1 (nivolumab or pembrolizumab), or combination ipilimumab plus nivolumab (*SI Appendix, Table S1*). A small number of normal donor peripheral blood samples were also analyzed in each batch as reference samples to enable the assessment and correction of technical batch effects (*Methods* and *SI Appendix, Fig. S3 A and B*).

First, we investigated whether immune checkpoint blockade therapies preferentially engage already activated T cells. Manual gating revealed a strong enrichment of Ki-67⁺ proliferative cells in PD-1⁺ versus PD-1⁻ CD8 T cells following anti-PD-1 monotherapy (Fig. 3A), consistent with prior observations (33, 34). This aligns with the notion that only already activated T cells expressing PD-1 would be sensitive to anti-PD-1 therapy. Interestingly, however, a similar effect was observed in patients who had received ipilimumab monotherapy (Fig. 3A). It is unclear whether this effect of anti-CTLA-4 therapy is due to modulation of already activated PD-1-expressing T cells or activation of resting T cells that subsequently up-regulate PD-1. Most notably, the frequencies of Ki-67⁺ cells were comparably elevated in both PD-1⁻ and PD-1⁺ CD8 T cells following combination ipilimumab plus nivolumab

therapy, consistent with our preclinical findings (Fig. 3A). This suggests that monotherapies are sufficient to induce the proliferation of already activated PD-1⁺ CD8 T cells and combination therapy is able to induce the proliferation of PD-1⁺ and PD-1^{low} CD8 T cells. In addition, manual gating revealed trends in the frequency of total CD4 and CD8 T cells consistent with engagement of CD8 and CD4 by anti-PD-1 and anti-CTLA-4, respectively (*SI Appendix, Fig. S4 A and B*). Combination therapy led to an increase in the overall frequency of CD8 T cells compared with anti-PD-1 monotherapies. In contrast, the frequency of CD4 T cells was increased in the blood of patients treated with ipilimumab compared with those treated with anti-PD-1 therapy. Interestingly, the frequency of Ki-67⁺ CD4 T cells in peripheral blood was not different between treatments, in contrast to the observed effects on CD8 T cells (*SI Appendix, Fig. S4C*).

To precisely delineate T cell populations that respond to therapy, a similar metaclustering approach was utilized. PD-1 and CTLA-4 were not used as parameters for clustering to exclude the possibility that staining can be inhibited by receptor occupancy following therapy, as has been observed previously in the context of anti-PD-1 therapy (33). Twenty-four T cell metaclusters were identified in peripheral blood samples, including 8 CD8 and 15 CD4 T cell subsets (*Methods, Fig. 3 B–D, and SI Appendix, Fig. S4 D and E*). Although anti-CTLA-4 treatment can induce ADCC in murine models, treatment with ipilimumab did not appear to lead to decreased Treg relative frequencies (Fig. 3D, metacluster 7). This may be attributed to differences in the effects on peripheral blood, but is consistent with a recent report that ipilimumab does not deplete Tregs (24). How these findings can be reconciled with prior findings that high-affinity Fc receptor allelic variants are associated with improved responses to anti-CTLA-4 therapy remains to be clarified (36). Recent findings that engagement of anti-CTLA-4 antibodies by Fcγ receptors can modulate T cell responses to therapy independent of Tregs may explain these findings in part (37).

Treatment-dependent associations with subset frequencies were observed in the CD8 and CD4 effector compartments. The frequency of a terminally differentiated TBET⁺ EOMES⁺ CD8 T cell subset was significantly increased in blood samples from patients receiving combination therapy compared with those receiving monotherapies (Fig. 3C, metacluster 1). Furthermore, metacluster 1 is more frequent in posttherapy samples versus in unmatched pretherapy samples (*SI Appendix, Fig. S4F*). Surprisingly, no significant changes in the frequency of PD-1⁺ CD8 T subsets (e.g., metacluster 16) were observed. These observations suggest that while monotherapies are sufficient to increase the proliferation of activated CD8 T cells (Fig. 3A), combination therapy is sufficient to also increase the frequency of terminally differentiated effector CD8 T cells. Supportive of this, monotherapies only led to increased Ki-67⁺ frequencies in PD-1⁺ CD8 T cells, whereas combination therapy led to similar Ki-67⁺ frequencies in PD-1⁺ and PD-1⁻ CD8 T cells (Fig. 3A).

Three CD4 effector populations were elevated following therapies containing anti-CTLA-4. The frequencies of activated CD45RO⁺ and CD45RO⁺ TBET⁺ EOMES⁺ CD4 effector T cell subsets were higher following ipilimumab compared with anti-PD-1 monotherapy (Fig. 3D, metaclusters 3 and 8, respectively). In addition, the frequency of a CD45RO⁺ ICOS⁺ PD-1⁺ CD4 effector T cell subset was higher in patients receiving ipilimumab than in patients receiving anti-PD-1 monotherapy or combination therapy (Fig. 3D, metacluster 19). This observation is consistent with prior observations that anti-CTLA-4 therapy leads to expansion of ICOS⁺ CD4 effector T cells (38–41); however, it remains unclear why a similar elevated frequency is not observed in the peripheral blood of combination therapy-treated patients.

Systematic Characterization of the Relationship Between T Cell Populations in the TME versus Those in Peripheral Blood. A key question is how closely changes in cellular frequencies in

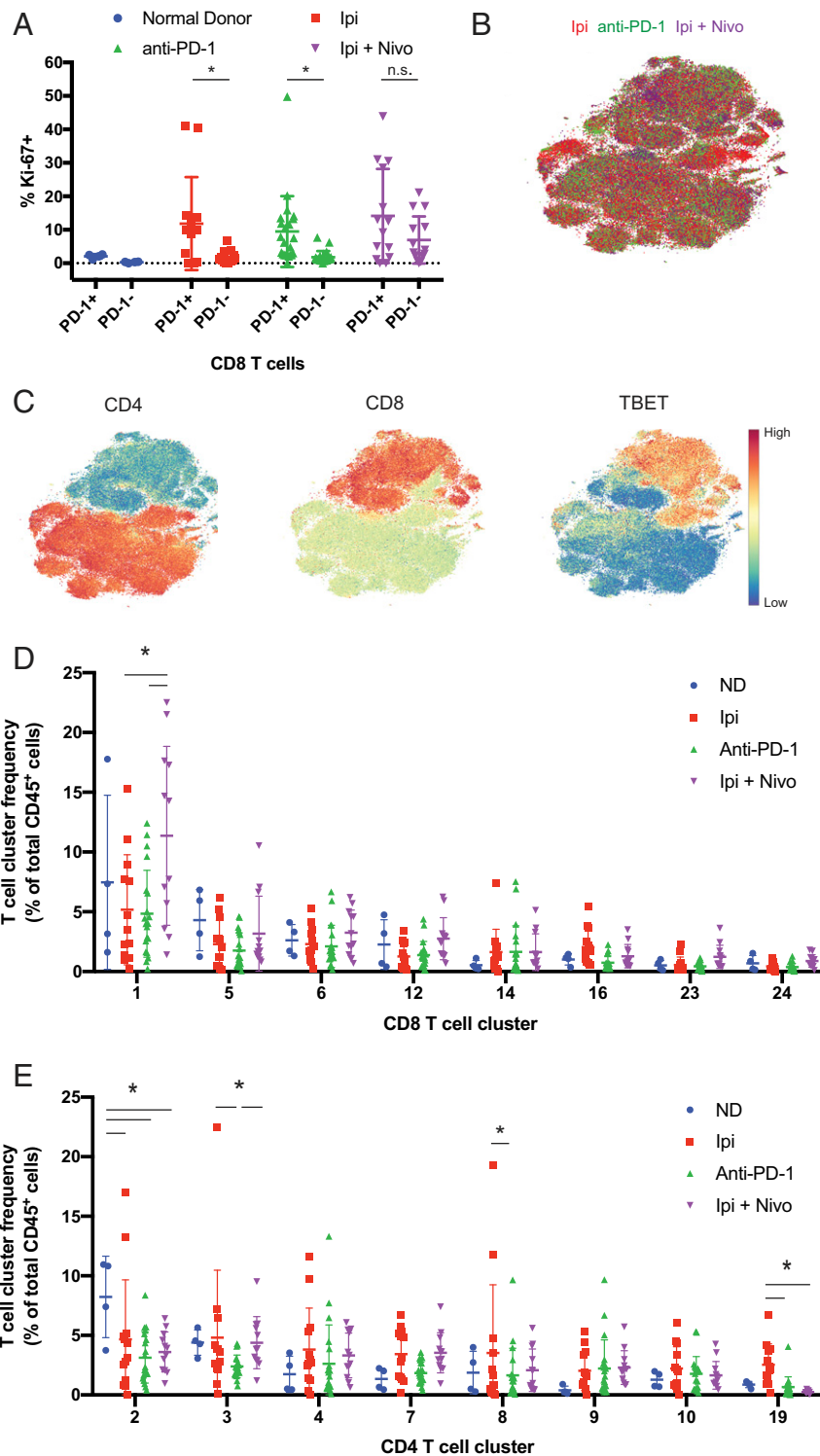


Fig. 3. Mass cytometry analysis of peripheral blood from patients treated with checkpoint blockade reveals treatment-specific effects. (A) Frequency of Ki-67⁺ cells within PD-1⁻ and PD-1⁺ fractions of CD8 T cells in peripheral blood from patients treated with checkpoint blockade therapies (anti-CTLA-4, ipilimumab [Ipi], anti-PD-1 monotherapy, and ipilimumab plus nivolumab [Ipi + Nivo]) and normal donors is displayed. **P* < 0.05, 1-way ANOVA with Sidak's multiple testing correction. n.s., not significant. (B) tSNE plot of T cells from peripheral blood from patients treated with checkpoint blockade therapies. The plot is color-coded by treatment. Equal numbers of events per treatment group are displayed. (C) tSNE plots of T cells from peripheral blood overlaid with the expression levels of CD4, CD8, and TBET as heat maps. (D) Frequency of CD8 T cell metaclusters identified in peripheral blood from normal donors and patients treated with monotherapy and combination checkpoint blockade therapy. **P* < 0.05 Tukey's 2-way ANOVA with multiple testing correction. The mean and SD are displayed for each frequency plot. ND, normal donor. (E) Frequency of CD4 effector T cell metaclusters identified in peripheral blood from normal donors and patients treated with monotherapy and combination checkpoint blockade therapy. **P* < 0.05, Tukey's 2-way ANOVA with multiple testing correction. (See also *SI Appendix, Figs. S3 and S4.*)

peripheral blood reflect changes in T cell frequencies within the TME. It is generally recognized that the phenotypes of tumor-infiltrating and peripheral blood lymphocyte populations are quite different; however, the extent of phenotypic and functional overlap remains ill-defined. We sought to apply a mass cytometry-based approach to systematically characterize relationships between the phenotypes and frequencies of such T cell populations in each tissue. To investigate the degree to which phenotypically defined T cell populations in peripheral blood reflect intratumoral T cell populations, we analyzed a publicly available mass cytometry dataset of matched lung tumors, normal adjacent lungs, and peripheral blood (20). This matched analysis approach enables assessment of the relative anatomical distribution of phenotypically defined T cell populations. A total of 21 T cell metaclusters were identified with 8 CD8 and 9 CD4 T cell populations (Fig. 4A).

Although many phenotypically defined T cell populations were identified in all tissues, several metaclusters were tissue-specific (Fig. 4B and C). Tumor-infiltrating T cell frequencies were more closely associated with T cell frequencies in normal adjacent lung than in peripheral blood. Although this observation is expected, it highlights a notable caveat to the identification and interpretation of tumor-infiltrating T cell populations. Although particular T cell populations may be present in tumor and not blood, they may not necessarily be directly relevant to the antitumor response but rather represent “bystander” tissue-resident populations. For example, the frequency of metacluster 7 in the tumor correlates with that in the normal adjacent lung, while it does not correlate with that in blood (and is present at low frequencies) (*SI Appendix, Fig. S5*). While resident T cell populations may play a significant role in antitumor immunity, this observation also raises the possibility that lung tissue-resident T cell populations may be present or even expand within the TME as “passengers” due to indirect effects.

Of interest were 1 CD8 and 2 CD4 effector populations that were present at significant frequencies in tumor but undetectable in blood (Fig. 4A and B, metaclusters 8, 14, and 18). The phenotypes of these subsets suggested active involvement in the antitumor response. The CD8 T cell subset displayed a PD-1⁺ LAG3^{int} TIM3^{int} phenotype (Fig. 4B, metacluster 18). This metacluster also displayed expression of CD39, which has been reported to be a marker of exhausted CD8 T cells in humans (42). Of the 2 CD4 T cell populations, metacluster 8 displayed an activated PD-1^{hi} ICOS^{int} CD39^{int} phenotype, while metacluster 14 displayed a PD-1^{int} CD127⁺ phenotype (Fig. 4A and B). These observations are consistent with the notion that T cells are exposed to chronic antigen stimulation within the TME and suggest that specific aspects of endogenous antitumor T cell responses can only be detected in tumor tissue. The presence of metacluster 8 but not metacluster 18 in normal adjacent lung tissue raises the possibility that metacluster 8 T cells are tissue resident-derived, while metacluster 18 arises from a systemic immune response. In addition, because these analyses are of treatment-naïve patients, the extent to which therapy-responsive populations can be detected remains unclear. These analyses indicate that while the bulk of T cell phenotypes are detectable in both peripheral blood and tumor samples, only a minority of subsets have a correlation between their frequencies in tumor and blood. These analyses also identify several populations for which frequencies in blood reflect intratumoral frequencies. These include an activated antigen D-related human leukocyte antigen-positive (HLA-DR⁺) CXCR3⁺ CD4 effector population and a CD45RA^{int} CD8 subset (Fig. 4A, metaclusters 1 and 3, respectively). Together, these findings support the utility of peripheral blood analyses, albeit limited in scope in treatment-naïve patients, but also indicate that analyses of peripheral blood alone cannot provide a complete characterization of antitumor immune responses.

Discussion

Here, we sought to determine whether combination anti-CTLA-4 plus anti-PD-1 therapy utilizes similar or distinct cellular mechanisms compared with monotherapies. These studies indicate that combination therapy effects on the frequencies of tumor-infiltrating and peripheral T cell populations are, in large part, similar to those of the constituent monotherapies, but also reveal distinct effects on phenotypically exhausted CD8 T cell populations. This indicates that dual blockade of CTLA-4 and PD-1 allows for engagement of divergent biological pathways in CD8 T cells. These findings are consistent with recent evidence that combination anti-CTLA-4 plus anti-PD-1 therapy leads to an expansion of both CD4 and CD8 CD45RO⁺ EOMES⁺ CD69⁺ T cells within the tumor (43). Importantly, our findings further define differential effects of combination therapy on phenotypically exhausted PD-1^{high} Lag3⁺ Tim3⁺ and activated effector PD-1⁺ Lag3^{int} Tim3^{int} CD8 T cells. These findings are in addition to additive effects of combination therapy on multiple CD4 and CD8 T cell subsets, including Th1-like CD4 effector T cells.

Overall, these findings provide insight into what mechanistic insights are required to guide rational design of combination immunotherapies. These findings suggest it is necessary to investigate the mechanisms of action of combination therapies rather than indirectly inferring such biology from the effects of monotherapies. Likewise, the known pharmacodynamics and biomarkers of response for monotherapies may not accurately reflect those of combination therapy. Larger and prospective clinical studies, as well as broader preclinical investigation, are warranted to further investigate these possibilities. Such mechanistic differences may make combination therapy more efficacious in the less immunogenic tumor types refractory to monotherapies. The enhanced efficacy of combination therapy in the context of renal cell carcinoma versus sunitinib supports this notion (9); however, the relative contribution of ipilimumab to the response rate in this context remains ill-defined, given emerging evidence that anti-PD-1 monotherapy has a relatively high response rate in the setting of renal cell carcinoma (44, 45).

A key outstanding question is what specific signaling pathways are differentially modulated by combination anti-CTLA-4 plus anti-PD-1 therapy in order to lead to the increase in frequency of activated effector PD-1⁺ Lag3^{int} Tim3^{int} CD8 T cells. Prior transcriptional analyses of murine tumor-specific CD8 T cells revealed that combination anti-CTLA-4 plus anti-PD-1 treatment leads to regulation of genes associated with effector function (12). Although the brief timing of our experimental model likely does not allow for the induction of a completely exhausted T cell state, as defined by adoption of exhaustion markers and decrease of functional output, the differential modulation of activated and phenotypically exhausted CD8 T cells by combination therapy raises several interesting possibilities. For example, combination therapy may be sufficient to attenuate the induction of a T cell exhaustion phenotype and/or associated reductions in functional output. Prior studies, however, reveal that the epigenetic state of exhausted CD8 T cells prevents a stable reversion by anti-PD-1 monotherapy (29, 30). If combination therapy can prevent, attenuate, or potentially reverse the induction of T cell exhaustion, this would have significant therapeutic implications.

Another related open question is which functional aspects of the antitumor response are modulated by combination therapy. Specifically, it is unclear whether combined checkpoint blockade enhances the magnitude of responses (e.g., increased killing capacity of CD8 effector T cells), alters the nature of antitumor immune responses (e.g., types of cytokines), or both, relative to checkpoint blockade monotherapies. Our studies here indicate that anti-CTLA-4 and combination therapy, but not anti-PD-1 monotherapy, leads to an expansion of CD4 effector T cells. This does not indicate that CD4 effector T cells are unnecessary for effective antitumor T cell responses in the context of PD-1 blockade

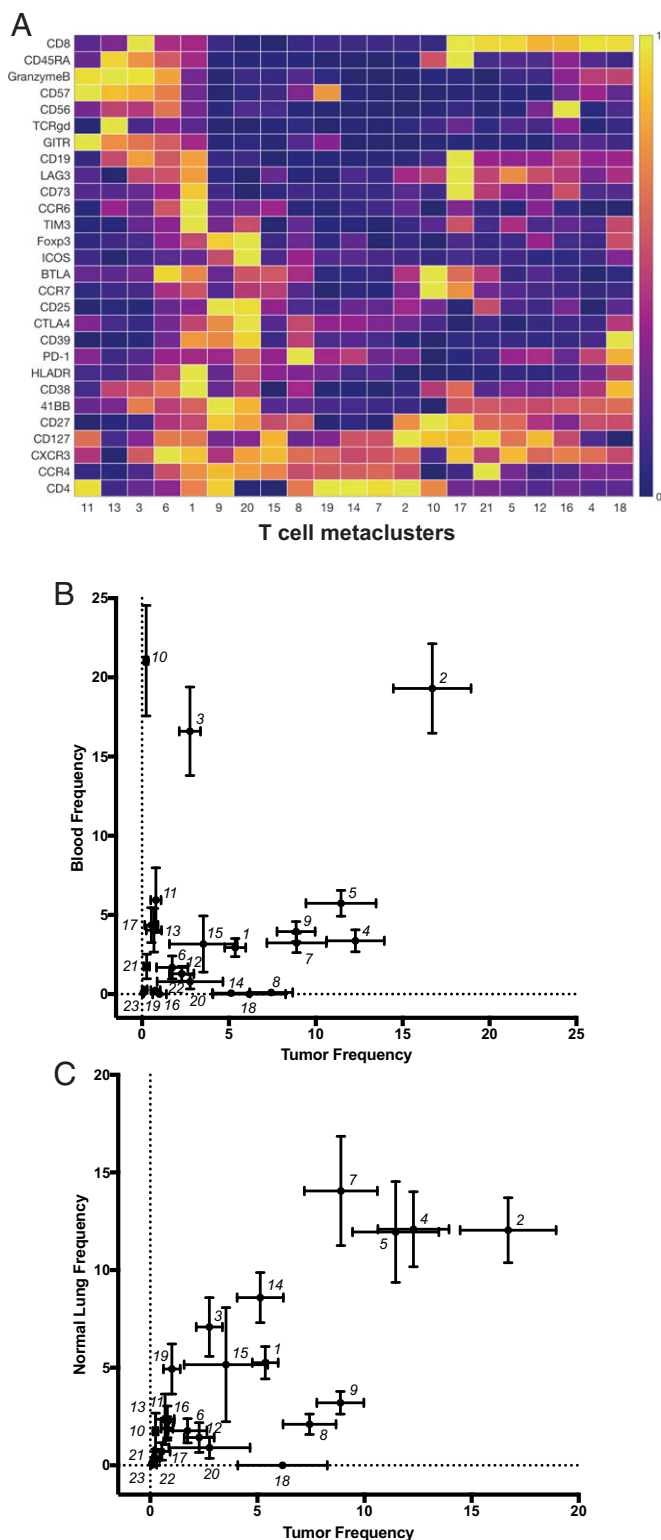


Fig. 4. Specific subsets of phenotypically defined T cell populations within the TME are detectable in peripheral blood of treatment-naive patients. (A) Heat map of T cell metaclusters identified across matched human lung tumors, normal adjacent lung, and peripheral blood. Expression values of individual parameters are normalized to the maximum mean value across metaclusters. (B) Mean frequency of T cell metaclusters in blood plotted as a function of their respective frequencies in tumor tissue. Interpatient variability is displayed within each tissue as the SE. Metacluster clusters are annotated. (C) Mean frequency of T cell metaclusters in normal adjacent lung plotted as a function of their respective frequencies in tumor tissue. (See also *SI Appendix, Fig. S5*.)

alone, but that PD-1 blockade does not enhance the endogenous CD4 effector response. The direct functional consequence of Th1-like CD4 effector T cell expansion following anti-CTLA-4 monotherapy and combined anti-CTLA-4 and anti-PD-1 therapy remains unclear. Recent evidence indicates that enhancement of CD4 effector function by combination blockade leads to increased activation of CD103⁺ dendritic cells (46). In addition, based on insights from viral systems, Th1 CD4 helper T cells may enhance CD8 T cell infiltration (47), enhance antibody penetration (48), enhance T cell memory formation, or have direct cytolytic capability as has been previously observed with tumor-specific CD4 T cells in the context of adoptive cell transfer (49). Another intriguing possibility is that CD4 T cells may employ cytokine-mediated killing of tumor cells rather than engaging in direct cytotoxicity. In addition, recent findings reveal that immune checkpoint blockade induces profound changes in specific myeloid subsets. These changes are most striking in the context of combination anti-CTLA-4 plus anti-PD-1 therapy and are partially dependent on IFN- γ (50). This raises the possibility that indirect modulation of tumor-infiltrating myeloid subsets by IFN- γ -producing CD8 and Th1-like CD4 effector T cells may represent part of the mechanism of combination therapy. Consistent with this notion, loss of negative costimulation releases limits on T cell differentiation, with genetic loss of CTLA-4 leading to emergence of noncanonical CD4 T cell phenotypes with elevated polyfunctional cytokine expression, including IFN- γ (25).

Understanding whether combination therapies utilize similar mechanisms as monotherapies is further important for determining whether combination therapies exhibit drug independence. Prior reports have suggested that most drug combinations, including ipilimumab plus nivolumab, derive their benefit through drug independence rather than additivity (51). These analyses were based on short-term follow-up of phase III clinical trial data, and further investigation in the context of long-term follow-up is clearly warranted. The contributions of drug independence and drug additivity are not completely mutually exclusive possibilities, and may both contribute to the enhanced efficacy of combination therapy. These possibilities highlight the need for further mechanistic investigation of monotherapies and combination therapies in both preclinical models and clinical samples. In summary, our findings here indicate that combination immune checkpoint blockade therapy induces distinct biological effects that manifest in different cellular changes in T cell populations.

Methods

Mice and In Vivo Murine Tumor Experiments. Seven-week-old female C57BL/6J mice were purchased from The Jackson Laboratory and allowed to acclimate in the housing facility for at least 1 wk prior to the initiation of tumor experiments. A previously empirically defined experimental system was utilized for MC38 tumor experiments (15). Briefly, 4×10^5 MC38 tumor cells suspended in 100 μ L of phosphate-buffered saline (PBS) were injected subcutaneously on the flank of mice. Immune checkpoint blockade antibodies (polyclonal hamster and rat IgG2a isotype [BioXCell], anti-CTLA-4 [clone 9H10; BioXCell], anti-PD-1 [RMP1-14; BioXCell], or combination anti-CTLA-4 plus anti-PD-1) were injected intraperitoneally 5, 8, and 11 d following tumor injection. Hamster polyclonal and anti-CTLA-4 antibodies were administered using doses of 200 μ g for the initial injection and 100 μ g for subsequent injections. Anti-PD-1 and rat isotype antibodies were administered at a dose of 250 μ g per injection. Mice were randomized to treatment groups prior to the first treatment dose. For short-term IdU experiments, 100 μ L of 5 mg/mL IdU (Sigma-Aldrich) in PBS was administered by intraperitoneal injection 30 min prior to euthanasia. Tumors were measured by digital caliper 2 to 3 times per week, with tumor volume calculated as volume = length \times width \times height. Mice were euthanized using CO₂ and subsequent cervical dislocation at the time of euthanasia for analysis. All animal experiments were performed in accordance with The University of Texas MD Anderson Cancer Center (MDACC) Institutional Animal Care and Use Committee (IACUC) guidelines in an MDACC American Association for Accreditation of Laboratory Animal Care (AAALAC)-accredited barrier facility vivarium.

Cell Lines. MC38 was grown as previously described (15, 52). Briefly, MC38 murine colon carcinoma cells were originally obtained from N. Restifo,

National Cancer Institute, Bethesda, MD; cultured in Dulbecco's modified Eagle's medium supplemented with 10% fetal bovine serum and penicillin and streptomycin; and periodically tested for *Mycobacterium* contamination. MC38 was derived from a female C57BL6 mouse. Cell lines were previously analyzed using whole-exome sequencing to interrogate mutational load (15), but have not been further authenticated by other approaches.

Human Subjects. Peripheral blood samples were from patients treated at The University of Texas MDACC between December 2011 and May 2017. All samples were obtained with patient informed consent, deidentified, and then analyzed under The University of Texas MDACC Institutional Review Board-approved protocols and in accordance with the Declaration of Helsinki. Clinical annotation data are displayed in *SI Appendix, Table S1*. Normal donor blood samples were collected from the Gulf Coast Blood Bank. Protected health information (PHI) is protected under The University of Texas MDACC PHI policy ADM0396. Patient age and gender information are not disclosed accordingly. Because normal donor blood samples were primarily used as reference samples (biological and technical) to ensure consistency across multiple acquisition batches, the donor samples are the same as in prior cohorts analyzed (15).

Mass Cytometry Antibodies. Metal-conjugated antibodies were either purchased from Fluidigm or conjugated in-house using X8 polymer kits per the manufacturer's protocol as previously described (15). Antibody, metal conjugate, and clone information is detailed in *SI Appendix, Tables S2 and S3*.

Mass Cytometry Sample Preparation and Data Acquisition. MC38 murine tumors were isolated from mice treated with control or checkpoint blockade antibodies and killed 13 d after tumor inoculation. Tumor tissue was isolated, processed, and stained with mass cytometry antibodies as previously described (15). Briefly, following manual dissociation, tumor samples were enzymatically digested with Liberase TL (Roche) and DNase I (Roche) for 30 min at 37 °C. Single-cell suspensions were generated by mashing digested tumors through 70- μ m filters and purified using a Histopaque-1119 (Sigma-Aldrich) discontinuous gradient on RPMI cell culture media centrifuged at 2,000 rpm for 20 min. Up to 2.5×10^6 cells were washed with fluorescence-activated cell sorting (FACS) buffer and then incubated with 2% of each bovine, murine, rat, hamster, and rabbit serum in PBS with 25 μ g/mL 2.4G2 antibody at 4 °C for 10 min prior to surface staining with an antibody mixture at 4 °C for 30 min in a 50- μ L volume. A 50- μ L volume of 2 \times solution of 194Pt monoisotopic cisplatin (Fluidigm) in PBS was added directly to the samples for a final concentration of 2.5 μ M for 1 min. Samples were immediately washed twice with FACS buffer and labeled using palladium barcoding per the manufacturer's protocol. Samples were prepared for intracellular staining using a FOXP3 fix and permeabilization kit per the manufacturer's protocol (Thermo Fisher Scientific) and then stained for 30 min at room temperature. Following 2 washes with permeabilization buffer and FACS buffer, samples were fixed again using 1.6% paraformaldehyde in PBS supplemented with 100 nM iridium nucleic acid intercalator (Fluidigm). Following fixation, cells were washed twice with 0.5% bovine serum albumin (BSA) PBS and 0.1% BSA water, filtered, and resuspended in 0.1% BSA water. Barcoded samples were then analyzed using a Helios mass cytometer (Fluidigm).

For analysis of human peripheral blood, cryopreserved samples were thawed and immediately washed prior to additional processing. Samples were then purified on a Histopaque gradient prior to staining using a similar protocol as described above for murine tumor infiltrating lymphocytes (TILs). Surface and intracellular antibody staining panels are detailed in *SI Appendix, Table S3*.

Mass Cytometry Data Analysis. Mass cytometry flow cytometry standard (FCS) data files were concatenated and bead-normalized using Helios software (Fluidigm), debarcoded using Helios software or the cell debarcoder in MATLAB (53), and exported for downstream analysis. Total CD45⁺ or T cell populations were manually identified and exported using negative and positive gating strategies of lineage markers in FlowJo. T cell-gated data were not subsampled and were subjected to an arcsinh transformation with a cofactor of 4. Clustering and metaclustering were performed using the well-validated algorithm PhenoGraph (16). A metaclustering approach was used to identify MC38 tumor-infiltrating T cell populations using a Euclidean distance metric with $k = 30$ for initial cluster identification at the per mouse level

and a cosine distance metric with $k = 15$ for metacluster assignment across cohorts. A similar metaclustering approach with these variable values was used for identification of T cell populations in publicly available human lung tumor mass cytometry data and human peripheral blood data. For all clustering approaches, samples with fewer than 1,000 events were excluded from the analysis.

The human peripheral blood mass cytometry data were acquired in 4 batches consisting of analytical samples and technical controls (repeated sampling of cryopreserved normal donors). Comparison of controls across cohorts (runs) revealed a significant batch effect (*SI Appendix, Fig. S3 A, Left*). When we performed metaclustering agnostic of multiple parameters (including TIM3, HLA-DR, CD28, and CD8a) the observed batch effect was reduced (*SI Appendix, Fig. S3 A, Center and Right*), suggesting that these specific channels contributed to most of the technical batch effect. Upon further inspection, these 4 channels did not appear to have any significant flaw other than a batch effect (an apparent shift in the background, and thus average signal). This initial approach to mitigate the batch effect present in the data ameliorated much of the batch effect but precluded the use of these parameters in the assignment of clusters across cohorts.

In order to more systematically correct the observed batch effect across cohorts, we chose to measure z-score protein expression within each cohort separately. More precisely, we subtracted the cohort mean expression of all proteins from each cell (within that cohort) and divided the result by the cohort level SD of respective protein expression. This procedure results in the protein expression distribution across cohorts having the same mean (0) and the same variance (1) but does not alter it within cohort biological variances; therefore, this minimizes any technical batch effect between cohorts. For this, we utilized the *zscore* function in MATLAB.

Subsequent analyses such as tSNE and PhenoGraph were performed using similar default parameters. In the case of PhenoGraph clustering of human samples, $k = 30$ was used to construct the graph. To determine whether this procedure minimized the technical batch effect between cohorts, replicate normal donor samples between cohorts were compared. tSNE overlays between these samples, indicating that this procedure removed the technical batch effects (*SI Appendix, Fig. S3B*).

Heat maps were generated using MATLAB. Individual parameters were normalized to the maximal mean expression of each parameter across clusters such that for each parameter, 1 cluster displayed maximal expression. To help in interpretation of the data, only clusters over 1% frequency were plotted.

Analysis of Publicly Available Data. For the analysis of previously published mass cytometry data (20), FCS files were downloaded from the Flow Repository (<https://flowrepository.org>; repository ID: FR-FCM-ZY9M). Data were analyzed using PhenoGraph and FlowJo as described above.

Datasets. Mass cytometry data have been deposited in the Flow Repository (murine TIL data; repository ID: FR-FCM-ZYQQ) (54). Human peripheral blood data from patients being treated with immune checkpoint blockade therapies were also deposited in the Flow Repository (repository ID: FCM-FR-ZYQR) (55).

Statistics. Statistics were performed in Prism 7.0 (GraphPad). Tumor growth and cellular frequencies between 2 groups were compared using 2-tailed *t* tests with Welch's correction or 1-way ANOVA with Sidak's multiple testing correction. Cluster frequencies were compared using 2-way ANOVA with Tukey's multiple testing correction. Correlations were displayed with linear regression lines with Spearman's rank correlation.

ACKNOWLEDGMENTS. We thank Duncan Mak for providing expert advice related to mass cytometry analyses. This work was supported by Grant R1203 from Cancer Prevention and Research in Texas (to J.P.A.). J.P.A. is a co-director of the Parker Institute for Cancer Immunotherapy. S.C.W. was an MDACC Odyssey postdoctoral fellow and is currently an employee of Spotlight Therapeutics. J.P.A. is a cofounder of Jounce and Neon Therapeutics. M.C.A. is supported by a National Health and Medical Research Council of Australia C. J. Martin Early Career Fellowship (no. 1148680). Mass cytometry was performed at the MDACC Flow Cytometry and Cellular Imaging Core Facility, which is funded, in part, by National Cancer Institute Cancer Center Support Grant P30CA16672.

1. D. M. Pardoll, The blockade of immune checkpoints in cancer immunotherapy. *Nat. Rev. Cancer* **12**, 252–264 (2012).
2. S. L. Topalian, C. G. Drake, D. M. Pardoll, Immune checkpoint blockade: A common denominator approach to cancer therapy. *Cancer Cell* **27**, 450–461 (2015).
3. P. Sharma, J. P. Allison, The future of immune checkpoint therapy. *Science* **348**, 56–61 (2015).
4. J. Tang, A. Shalabi, V. M. Hubbard-Lucey, Comprehensive analysis of the clinical immuno-oncology landscape. *Ann. Oncol.* **29**, 84–91 (2018).

5. S. C. Wei, C. R. Duffy, J. P. Allison, Fundamental mechanisms of immune checkpoint blockade therapy. *Cancer Discov.* **8**, 1069–1086 (2018).
6. E. Hui et al., T cell costimulatory receptor CD28 is a primary target for PD-1-mediated inhibition. *Science* **355**, 1428–1433 (2017).
7. M. A. Curran, W. Montalvo, H. Yagita, J. P. Allison, PD-1 and CTLA-4 combination blockade expands infiltrating T cells and reduces regulatory T and myeloid cells within B16 melanoma tumors. *Proc. Natl. Acad. Sci. U.S.A.* **107**, 4275–4280 (2010).

8. J. Larkin *et al.*, Combined nivolumab and ipilimumab or monotherapy in untreated melanoma. *N. Engl. J. Med.* **373**, 23–34 (2015).
9. R. J. Motzer *et al.*; CheckMate 214 Investigators, Nivolumab plus ipilimumab versus sunitinib in advanced renal-cell carcinoma. *N. Engl. J. Med.* **378**, 1277–1290 (2018).
10. M. J. Overman *et al.*, Durable clinical benefit with nivolumab plus ipilimumab in DNA mismatch repair-deficient/microsatellite instability-high metastatic colorectal cancer. *J. Clin. Oncol.* **36**, 773–779 (2018).
11. M. Postow *et al.*, “Pooled 3-year overall survival data from phase II and phase III trials of nivolumab (NIVO) combined with ipilimumab (IPI) in advanced melanoma” in *32nd Annual Meeting and Pre-Conference Programs of the Society for Immunotherapy of Cancer (SITC 2017): Part One*, P. J. Romero, Ed. (Journal for Immunotherapy of Cancer, 2017), vol. 5, p. 86.
12. M. M. Gubin *et al.*, Checkpoint blockade cancer immunotherapy targets tumour-specific mutant antigens. *Nature* **515**, 577–581 (2014).
13. R. Das *et al.*, Combination therapy with anti-CTLA-4 and anti-PD-1 leads to distinct immunologic changes in vivo. *J. Immunol.* **194**, 950–959 (2015).
14. R. Das *et al.*, Early B cell changes predict autoimmunity following combination immune checkpoint blockade. *J. Clin. Invest.* **128**, 715–720 (2018).
15. S. C. Wei *et al.*, Distinct cellular mechanisms underlie anti-CTLA-4 and anti-PD-1 checkpoint blockade. *Cell* **170**, 1120–1133.e17 (2017).
16. J. H. Levine *et al.*, Data-driven phenotypic dissection of AML reveals progenitor-like cells that correlate with prognosis. *Cell* **162**, 184–197 (2015).
17. R. Melchionti, F. Gracio, S. Kordasti, A. K. Todd, E. de Rinaldis, Cluster stability in the analysis of mass cytometry data. *Cytometry A* **91**, 73–84 (2017).
18. B. Bengsch *et al.*, Epigenomic-guided mass cytometry profiling reveals disease-specific features of exhausted CD8 T cells. *Immunity* **48**, 1029–1045.e5 (2018).
19. S. Chevrier *et al.*, An immune atlas of clear cell renal cell carcinoma. *Cell* **169**, 736–749.e18 (2017).
20. Y. Lavin *et al.*, Innate immune landscape in early lung adenocarcinoma by paired single-cell analyses. *Cell* **169**, 750–765.e17 (2017).
21. T. R. Simpson *et al.*, Fc-dependent depletion of tumor-infiltrating regulatory T cells co-defines the efficacy of anti-CTLA-4 therapy against melanoma. *J. Exp. Med.* **210**, 1695–1710 (2013).
22. Y. Bulliard *et al.*, Activating Fc γ receptors contribute to the antitumor activities of immunoregulatory receptor-targeting antibodies. *J. Exp. Med.* **210**, 1685–1693 (2013).
23. M. J. Selby *et al.*, Anti-CTLA-4 antibodies of IgG2a isotype enhance antitumor activity through reduction of intratumoral regulatory T cells. *Cancer Immunol. Res.* **1**, 32–42 (2013).
24. A. Sharma *et al.*, Anti-CTLA-4 immunotherapy does not deplete FOXP3+ regulatory T cells (Tregs) in human cancers. *Clin. Cancer Res.* **25**, 1233–1238 (2018).
25. S. C. Wei *et al.*, Negative co-stimulation constrains T cell differentiation by imposing boundaries on possible cell states. *Immunity* **50**, 1084–1098.e10 (2019).
26. S. J. Im *et al.*, Defining CD8+ T cells that provide the proliferative burst after PD-1 therapy. *Nature* **537**, 417–421 (2016).
27. I. Siddiqui *et al.*, Intratumoral Tcf1(+)-PD-1(+)-CD8(+) T cells with stem-like properties promote tumor control in response to vaccination and checkpoint blockade immunotherapy. *Immunity* **50**, 195–211.e10 (2019).
28. D. T. Utzschneider *et al.*, T cell factor 1-expressing memory-like CD8(+) T cells sustain the immune response to chronic viral infections. *Immunity* **45**, 415–427 (2016).
29. K. E. Pauken *et al.*, Epigenetic stability of exhausted T cells limits durability of reinvigoration by PD-1 blockade. *Science* **354**, 1160–1165 (2016).
30. M. Philip *et al.*, Chromatin states define tumour-specific T cell dysfunction and reprogramming. *Nature* **545**, 452–456 (2017).
31. M. H. Spitzer *et al.*, Systemic immunity is required for effective cancer immunotherapy. *Cell* **168**, 487–502.e15 (2017).
32. S. Spranger *et al.*, Mechanism of tumor rejection with doublets of CTLA-4, PD-1/PD-L1, or IDO blockade involves restored IL-2 production and proliferation of CD8(+) T cells directly within the tumor microenvironment. *J. Immunother. Cancer* **2**, 3 (2014).
33. A. C. Huang *et al.*, T-cell invigoration to tumour burden ratio associated with anti-PD-1 response. *Nature* **545**, 60–65 (2017).
34. A. O. Kamphorst *et al.*, Proliferation of PD-1+ CD8 T cells in peripheral blood after PD-1-targeted therapy in lung cancer patients. *Proc. Natl. Acad. Sci. U.S.A.* **114**, 4993–4998 (2017).
35. C. Krieg *et al.*, High-dimensional single-cell analysis predicts response to anti-PD-1 immunotherapy. *Nat. Med.* **24**, 144–153 (2018).
36. F. Arce Vargas *et al.*, Fc effector function contributes to the activity of human anti-CTLA-4 antibodies. *Cancer Cell* **33**, 649–663.e4 (2018).
37. J. D. Waight *et al.*, Selective Fc γ R co-engagement on APCs modulates the activity of therapeutic antibodies targeting T cell antigens. *Cancer Cell* **33**, 1033–1047.e5 (2018).
38. N. Chaput *et al.*, Baseline gut microbiota predicts clinical response and colitis in metastatic melanoma patients treated with ipilimumab. *Ann. Oncol.* **28**, 1368–1379 (2017).
39. R. H. Vonderheide *et al.*, Tremelimumab in combination with exemestane in patients with advanced breast cancer and treatment-associated modulation of inducible costimulatory expression on patient T cells. *Clin. Cancer Res.* **16**, 3485–3494 (2010).
40. C. I. Liakou *et al.*, CTLA-4 blockade increases IFN γ -producing CD4+ICOShi cells to shift the ratio of effector to regulatory T cells in cancer patients. *Proc. Natl. Acad. Sci. U.S.A.* **105**, 14987–14992 (2008).
41. H. Chen *et al.*, Anti-CTLA-4 therapy results in higher CD4+ICOShi T cell frequency and IFN γ levels in both nonmalignant and malignant prostate tissues. *Proc. Natl. Acad. Sci. U.S.A.* **106**, 2729–2734 (2009).
42. P. K. Gupta *et al.*, CD39 expression identifies terminally exhausted CD8+ T cells. *PLoS Pathog.* **11**, e1005177 (2015).
43. T. N. Gide *et al.*, Distinct immune cell populations define response to anti-PD-1 monotherapy and anti-PD-1/anti-CTLA-4 combined therapy. *Cancer Cell* **35**, 238–255.e6 (2019).
44. B. I. Rini *et al.*; KEYNOTE-426 Investigators, Pembrolizumab plus axitinib versus sunitinib for advanced renal-cell carcinoma. *N. Engl. J. Med.* **380**, 1116–1127 (2019).
45. D. F. McDermott *et al.*, First-line pembrolizumab (pembro) monotherapy for advanced non-clear cell renal cell carcinoma (nccRCC): Results from KEYNOTE-427 cohort B. *J. Clin. Oncol.* **37**(suppl. 7), 546 (2019).
46. P. A. Beavis *et al.*, Dual PD-1 and CTLA-4 checkpoint blockade promotes antitumor immune responses through CD4(+)-Foxp3(-) cell-mediated modulation of CD103(+) dendritic cells. *Cancer Immunol. Res.* **6**, 1069–1081 (2018).
47. Y. Nakanishi, B. Lu, C. Gerard, A. Iwasaki, CD8(+) T lymphocyte mobilization to virus-infected tissue requires CD4(+) T-cell help. *Nature* **462**, 510–513 (2009).
48. N. Iijima, A. Iwasaki, Access of protective antiviral antibody to neuronal tissues requires CD4 T-cell help. *Nature* **533**, 552–556 (2016).
49. S. A. Quezada *et al.*, Tumor-reactive CD4(+) T cells develop cytotoxic activity and eradicate large established melanoma after transfer into lymphopenic hosts. *J. Exp. Med.* **207**, 637–650 (2010).
50. M. M. Gubin *et al.*, High-dimensional analysis delineates myeloid and lymphoid compartment remodeling during successful immune-checkpoint cancer therapy. *Cell* **175**, 1014–1030.e19 (2018).
51. A. C. Palmer, P. K. Sorger, Combination cancer therapy can confer benefit via patient-to-patient variability without drug additivity or synergy. *Cell* **171**, 1678–1691.e13 (2017).
52. A. van Elsland, A. A. Hurwitz, J. P. Allison, Combination immunotherapy of B16 melanoma using anti-cytotoxic T lymphocyte-associated antigen 4 (CTLA-4) and granulocyte/macrophage colony-stimulating factor (GM-CSF)-producing vaccines induces rejection of subcutaneous and metastatic tumors accompanied by autoimmune depigmentation. *J. Exp. Med.* **190**, 355–366 (1999).
53. E. R. Zunder *et al.*, Palladium-based mass tag cell barcoding with a doublet-filtering scheme and single-cell deconvolution algorithm. *Nat. Protoc.* **10**, 316–333 (2015).
54. S. C. Wei, N.-A. A. S. Anang, J. P. Allison, MC38 combination therapy. Flow Repository. <https://flowrepository.org/id/FR-FCM-ZYQQ>. Deposited 1 September 2018.
55. S. C. Wei, N.-A. A. S. Anang, M. C. Andrews, A. Reuben, A. P. Cogdill, J. A. Wargo, J. P. Allison, On-therapy PBMC samples. Flow Repository. <https://flowrepository.org/id/FR-FCM-ZYQR>. Deposited 1 September 2018.